

# Design Criteria for Patient-specific Mandibular Continuity Defect Reconstructed Implant with Lightweight Structure using Weighted Topology Optimization and Validated with Biomechanical Fatigue Testing

Chun-Li Lin<sup>1\*</sup>, Yu-Tzu Wang<sup>2</sup>, Chun-Ming Chang<sup>3</sup>, Cheng-Hsien Wu<sup>4</sup>, Wei-Heng Tsai<sup>1</sup>

<sup>1</sup>Department of Biomedical Engineering, National Yang Ming Chiao Tung University, Hsinchu, Taiwan

<sup>2</sup>Department of Mechanical and Electro-Mechanical Engineering, TamKang University, New Taipei City, Taiwan

<sup>3</sup>National Applied Research Laboratories, Instrument Technology Research Center, Hsinchu, Taiwan

<sup>4</sup>Department of Oral and Maxillofacial Surgery, Taipei Veterans General Hospital, School of Dentistry, National Yang Ming Chiao Tung University, Hsinchu, Taiwan

**Abstract:** This study developed design criterion for patient-specific reconstructed implants with appearance consideration and structural optimization of various mandibular continuity defects. The different mandible continuity defects include C (from left to right canines), B (from 1<sup>st</sup> premolar to 3<sup>rd</sup> molar), and A (from 3<sup>rd</sup> molar to ramus) segments defined based on the mandible image. The finite element (FE) analysis and weighted topology optimization methods were combined to design internal support beam structures within different reconstructed implants with corresponding occlusal conditions. Five continuity mandibular defects (single B/C/A+B and combination of B+C and B+C+B segments) were restored using additive manufacturing (AM) reconstructed implant and bone plate to confirm reasonable design criterion through biomechanical fatigue testing. The worst mandible strength was filtered based on the material mechanics and results from segmental bone length, thickness, and height statistics from the established database containing mandible images of 105 patients. The weighted optimization analysis results indicated that the sizes and positions of internal supporting beams within the reconstructed C, B, and A+B implants can be defined parametrically through corresponding segmental bone length, width, and height. The FE analysis found that the weight variation percentage between the parametric designed implants and original core solid implants in the C, B, and A+B was reduced by 54.3%, 63.7%, and 69.7%, respectively. The maximum stress values of the reconstructed implant and the remaining bone were not obviously reduced but the stress values were far lower than the material ultimate strength. The biomechanical fatigue testing indicated that all cases using the AM reconstructed implant could pass the 250,000 dynamic load. However, condyle head, bone plate fracture, and bone screw loosening could be found in cases using bone plates. This study developed a design criterion for patient-specific reconstructed implants for various mandibular continuity defects applicable for AM to further clinical use.

**Keywords:** Patient-specific implant; Mandibular continuity defect; Topology optimization; Finite element analysis; Additive manufacturing; Biomechanical testing

\*Correspondence to: Chun-Li Lin, National Yang Ming Chiao Tung University, Hsinchu, Taiwan; cllin2@nycu.edu.tw

**Received:** August 23, 2021; **Accepted:** October 18, 2021; **Published Online:** December 10, 2021

**Citation:** Lin CL, Wang YT, Chang CM, *et al.*, 2022, Design Criteria for Patient-Specific Mandibular Continuity Defect Reconstructed Implant with Lightweight Structure Using Weighted Topology Optimization and Validated with Biomechanical Fatigue Testing. *Int J Bioprint*, 8(1):437. <http://doi.org/10.18063/ijb.v8i1.437>

## 1. Introduction

The application integrating metal additive manufacturing (AM), medical image processing, and computer-aided

design (CAD) technologies to reconstruct patient-specific mandibular continuity defects are accepted to restore the patient appearance and mandible structural strength<sup>[1-11]</sup>. The subsequent combination of chemical

and radiotherapy in clinical practice has greatly improved the mandibular reconstruction surgery success rate<sup>[12]</sup>. However, current patient-specific mandibular continuity defect reconstructed implant designs are demanded for the following considerations. The structure must be optimized for lightweight design to reduce the weight of the large metal implant and withstand the physiological loads from chewing<sup>[11]</sup>. Micro-interfacial porous structures at the interface between the implant and the residual bone must also be considered to enhance osseointegration for bonded strength to improve the overall restored mandible structural stiffness<sup>[11,13,14]</sup>. Future complex post-operative dental prostheses that are built based on the long-term surgery success rate are essential to greatly enhance quality of life<sup>[6,9,11,12]</sup>.

Mandibular continuity defects may occur in different regions accompanied with complicated occlusal forces based on patient-specific consideration<sup>[18]</sup>. The effective structural lightweight optimization analysis should be theoretically targeted at specific reconstructed implant contours and load conditions to generate the most effective structure. However, a huge gap in design and manufacture induces the lack of clinical efficiency applicability because practical patient-specific optimization analysis is a time-consuming and difficult task.

According to the Food and Drug Administration (FDA) substantial equivalence (SE) definition, the functional fatigue mechanical performance of reconstructed AM implants must be compared to traditional reconstruction bone plates based on the same indications, implant material, and bone segments<sup>[15]</sup>. However, it may not be possible to perform fatigue testing immediately before clinical use when considering only one patient's structural appearance and segment design. Therefore, it is impossible to comply with the FDA's requirements for SE comparison for functional fatigue testing.

In addition to performing the pre-clinical testing listed in the product regulatory code according to the FDA's inspection and registration requirements for patient-specific implants, it is necessary to define the applicable dimension range of the patient-specific product and its corresponding functionality testing of the structural worst case to ensure safe and effective surgical results<sup>[15]</sup>. When the mandibular continuity defects can be designed within the classification and effective size range, building a mandibular continuity defect reconstructed implant with patient-specific contours and segmental parameterized structure design can be a great benefit to precise personal treatment.

This study developed design criterion for generating patient-specific reconstructed mandibular implants with contour consideration and structural optimization. Different large-scale mandible defects

are defined based on the worst mechanical strength mandible filtered from the established database of mandible images. The finite element (FE) analysis and weighted topology optimization methods were combined to design reconstructed implants for different mandibular continuity defects with corresponding occlusal conditions from the worst mandibular case. Further post-operative dental prostheses concerns for the reconstructed implant can be considered in the design criteria. Each possible combination reconstructed implant was fabricated using the AM technique. Biomechanical fatigue testing was performed to carry out reasonable designs.

## 2. Materials and methods

### 2.1. Mandible image database establishment and definition of the worst structure case

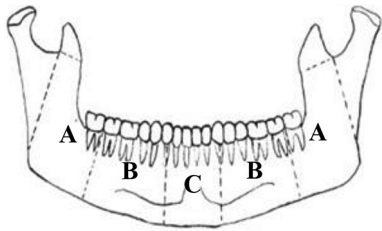
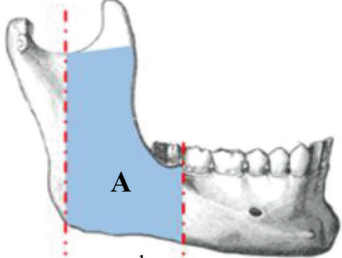
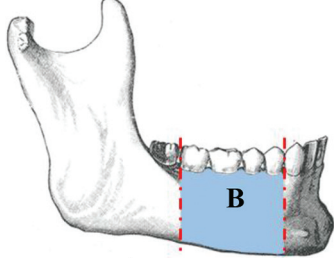
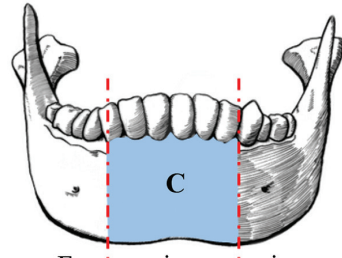
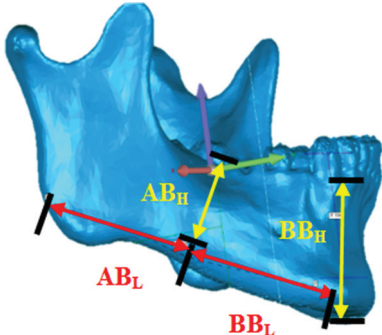
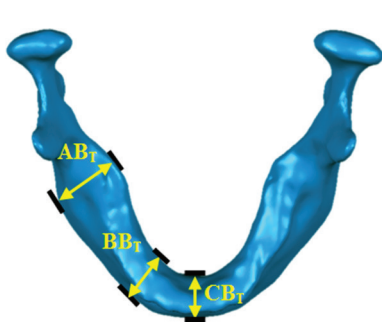
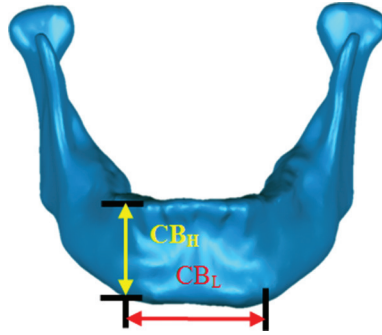
A total of 105 sets of normal mandibular computed tomography (CT) medical image Digital Imaging and Communications in Medicine (DICOM) files, including facial medical imaged patient skulls aged 20–65 years, were collected in this study and approved by the Ethics Committee (the Institutional Review Board; IRB) of Taipei Veterans General Hospital, Taiwan (Measurement and statistical analysis of Taiwanese mandibular size; approval number: 2019-01-050BC). All mandible DICOM images were processed to identify contours and a three-dimensional (3D) reconstructed image model of the mandible bone. According to the symmetry characteristics, the mandible can be divided into three segments (A, B, and C) and their corresponding length, width, and height measured according to the definitions in **Table 1**. After measuring the length/height/thickness of each segment from 105 CT images, a CT image with the weakest mandibular structure was selected as the worst case using V value calculation. This model was used as the standard model for patient-specific implant design for each mandible segment. The V value of each patient was calculated using Equation 1:

$$V = (AB_{Li} - AB_{L,ave}) + (BB_{Li} - BB_{L,ave}) + (CB_{Li} - CB_{L,ave}) + [- (AB_{Hi} - AB_{H,ave})] + \dots + [- (CB_{Ti} - CB_{T,ave})] \quad (1)$$

where  $i=1-105$  patients;  $AB_{L,ave}$ ,  $AB_{H,ave}$ ,  $AB_{T,ave}$ ,  $BB_{L,ave}$ ,  $BB_{H,ave}$ ,  $\dots$ ,  $CB_{T,ave}$ , indicating the average bone length, height, and thickness for A, B, and C segments obtained from all patients, respectively.

Taking the A+B bone segment as an example and simplified into a cantilever beam and fixed at the distal side (**Figure 1**), the minimum bone stress ( $\sigma$ ) occurred

**Table 1.** Definitions of individual length, height, and width definitions for mandibular segment A, B, and C and their corresponding length, width, and height.

	Symbol	Definition	Detail description
	AB <sub>L</sub>	Length of segment A	The arc length of the inferior border of the angle and ramus (from third molar to the masseteric tuberosity)
	AB <sub>T</sub>	Thickness of segment A	The maximum width of the angle and ramus
	AB <sub>H</sub>	Height of segment A	The height of the angle and ramus
	BB <sub>L</sub>	Length of segment B	The arc length of the inferior border of the body (from first premolar to second molar)
	BB <sub>T</sub>	Thickness of segment B	The maximum width of the body
	BB <sub>H</sub>	Height of segment B	The height of the body
	CB <sub>L</sub>	Length of segment C	The arc length of the inferior border of the symphyseal and parasymphyseal (from canine to canine)
	CB <sub>T</sub>	Thickness of segment C	The maximum width of the symphyseal and parasymphyseal
	CB <sub>H</sub>	Height of segment C	The height of the symphyseal and parasymphyseal
 From 3 <sup>rd</sup> molar to ramus	 From 1 <sup>st</sup> premolar to 3 <sup>rd</sup> molar	 From canine to canine	
			

when the beam received the smallest bending moment ( $M=F \times LB$ ) and presents the largest cross-sectional area, that is, the length (LB) is the shortest, the thickness (TB) is the thickest, and the height (HB) is the highest according to the bending stress equation from the material mechanics<sup>[16]</sup>. The bone length (LB) was set to a positive value, and the thickness (TB) and height (TH) were set to a negative value. A larger V value obtained from Equation 1 indicates a longer bone segment, as well as and shorter (smaller cross-sectional area) bone. This means that the bone segment structural strength is weaker. Conversely, bone structural strength is safer when V has a

smaller value. The V value was found between 13.71 and -25.74 based on the calculation results from 105 patients (Table 2). Five cases with the largest V values were selected as the cases with the weakest mechanical strength based on the images from all patients (Table 3).

To avoid the selected V value from being affected by the extreme value of a single size, the Z<sub>j</sub> value represented the relationship between the variation between each feature size and its average value and the standard deviation calculated to understand the variations in each feature size. The average and standard deviation (SDZ) of the 9 Z<sub>j</sub> values can be further calculated and

used to filter the influence of a certain feature size with a maximum or minimum value (Table 3).

$$Z_j = \frac{j - j_{ave}}{sd_j} \text{ where, } j = AB_L, BB_L, \dots, CB_T \quad (2)$$

$$SDZ = \sqrt{\frac{\sum_{j=1}^{n=9} (Z_j - \bar{Z})^2}{(n-1)}} < 1.00 \quad (3)$$

Where, sd value is one of the nine segmental bone length, width, and height dimensions.

The worst mandible structure case, that is, the structural weakest case can be filtered through calculating the V and SDZ values. The mandible with the largest V value and SDZ value definition <1.0 was the worst case, and their corresponding values were 13.71 and 0.66, respectively (Table 3).

### 2.2. Design criteria for reconstructed implant with large defect segment

Solid models of A, B, and C regions according to the definitions in Table 1 were constructed and divided in the CAD system (Creo Parametric v2.0, PTC, Needham, MA, USA) based on the previously selected worst mandible structure. Large mandible defects including single segment C and B and combined A+B segment were defined and designed with corresponding reconstructed implants according to the following five design points: (i) The thickness of the implant shell was set to 0.5 mm; (ii) the height of the implant was designed to be 1/2 of the height of the bone segment, and the bone graft space for postoperative prosthesis is reserved at the top for subsequent follow-up; (iii) the thickness of the implant was designed to be 2/3 of the bone segment thickness to allow space for the flap, vascular pedicle, and soft tissue to pass through; (iv) the implant needs to be designed with an extended side wing with a thickness of 2.8 mm, and 3-5 holes were reserved to provide 2.4 mm bone screws for fixation; and (v) the implant edges were rounded to prevent sharp edges and corners that damage

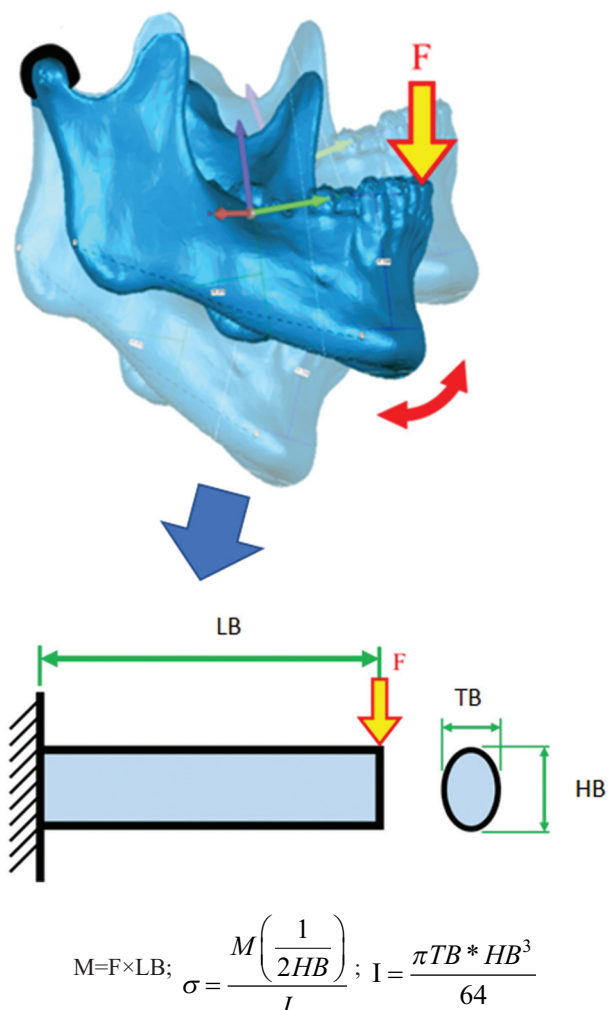


Figure 1. Mandibular occlusion simplified into material mechanics cantilever beam. M, F, LB, TB, and HB are the bending moment, occlusal force, bone length, thickness, and height, respectively. The  $\sigma$  represents the bending stress and I is the second moment inertia.

Table 2. Some representative average length, height, thickness, and V values obtained from Equation 1 and indicated safest and worst cases.

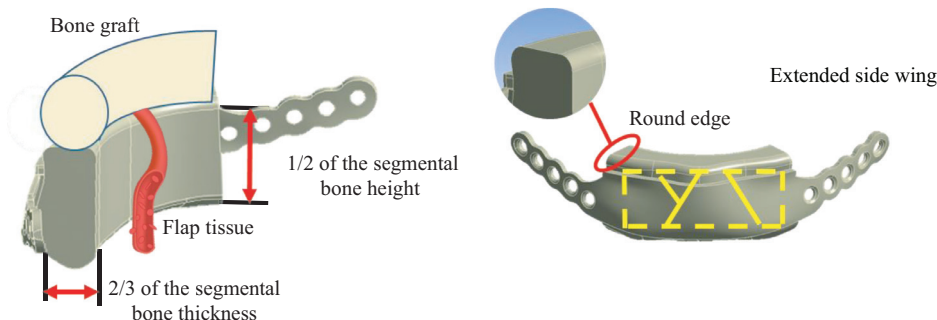
Case no.	AB <sub>L</sub>	BB <sub>L</sub>	CB <sub>L</sub>	AB <sub>H</sub>	BB <sub>H</sub>	CB <sub>H</sub>	AB <sub>T</sub>	BB <sub>T</sub>	CB <sub>T</sub>	V
1	26.42	48.17	35.82	23.83	30.21	32.61	16.00	11.40	12.92	3.54
2	39.99	50.18	34.01	33.19	31.97	31.08	16.97	13.49	16.45	1.14
...	...	...	...	...	...	...	...	...	...	...
105	33.87	48.71	40.34	25.43	30.42	34.24	12.60	11.28	11.56	17.51
Worst case										13.71
Safest case										-25.74
Ave.	AB <sub>L,ave</sub>	BB <sub>L,ave</sub>	CB <sub>L,ave</sub>	ABH <sub>ave</sub>	BBH <sub>ave</sub>	CBH <sub>ave</sub>	ABT <sub>ave</sub>	BBT <sub>ave</sub>	CBT <sub>ave</sub>	
	34.53	45.01	36.81	27.71	29.91	30.82	17.74	14.57	15.70	
SD (sd <sub>j</sub> )	4.88	4.61	2.94	3.27	2.44	2.92	2.16	2.59	2.09	

**Table 3.** Top five worst cases and corresponding  $Z_j$  and SD values.

Top five worst cases	V	$Z_{ABL}$	$Z_{BBL}$	$Z_{CBL}$	$Z_{ABH}$	$Z_{BBH}$	$Z_{CBH}$	$Z_{ABT}$	$Z_{BBT}$	$Z_{CBT}$	SDZ value	$SDZ \leq 1.0$
1	17.51	-0.13	0.80	1.20	0.70	-0.21	-1.17	2.38	1.27	1.98	1.06	X
2	15.43	0.48	-0.32	-1.02	2.21	0.96	0.26	1.99	0.10	1.27	1.00	X
3	13.71	-0.44	1.16	1.78	0.14	0.79	-0.08	-0.02	0.58	0.79	0.66	O (worst case)
4	12.31	0.15	0.72	0.88	1.21	-0.29	-0.32	0.39	0.31	0.82	0.49	O
5	12.14	0.62	0.58	1.04	0.66	1.54	0.25	0.06	-0.15	-1.41	0.78	O

**Table 4.** Main dimensions of C, B, and A + B reconstructed implants.

Implant C		Implant B		Implant A + B	
L	43.0	L	46.0	D	Ø 2.6
D	Ø 2.6	D	Ø 2.6	H1	18.0
H	17.7	H	19.0	H2	15.0
T1	8.4	T1	7.6	H3	34.0
T2	2.8	T2	2.8	T1	7.6
Unit: mm				T2	2.8



**Figure 2.** Clinical design consideration of a reconstructed implant in large defect segment.

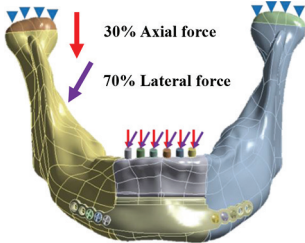
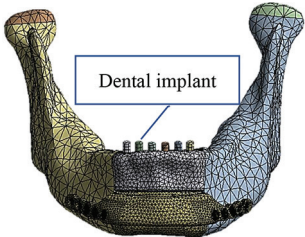
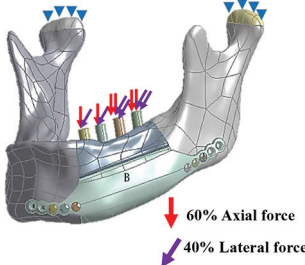
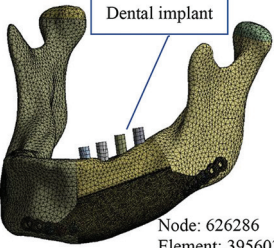
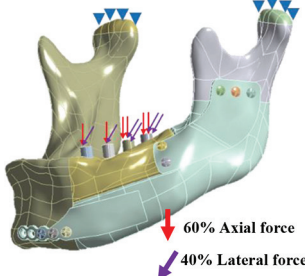
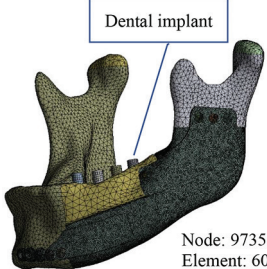
the soft tissues such as blood vessels (**Figure 2**). **Table 4** shows the reconstruction implant C, B, and A+B main dimensions.

**2.3. FE and weight topology optimization analysis**

Solid models of B, C, and A+B reconstructed implants and corresponding fixation screws, bone graft, and remaining bones were exported into ANSYS Workbench (ANSYS Workbench v18.2, ANSYS Inc., PA, USA) for simulation. Six-cylinder solid dental implants designed in

a CAD system with 3 mm diameter and 15 mm length aligned to the left/right canine, side incisor and incisor positions, and four other implants with 4.5 mm diameter and 14 mm length aligned to the 1<sup>st</sup>/2<sup>nd</sup> premolar and molar positions were inserted into C and B/A+B segmental bone grafts, respectively. These implants were used to simulate the post-operative prosthesis to receive corresponding occlusal loads. Three FE models were generated using quadratic 10-node tetrahedral structural solid elements after mesh convergence tests (**Table 5**).

**Table 5.** Solid and FE models of mandibular defect restored with C, B, and A+B reconstructed implants and corresponding bone grafts and dental implants.

Segment	Solid model	FE mesh model
C		 Node: 206661 Element: 120478
B		 Node: 626286 Element: 395603
A+B		 Node: 973534 Element: 607069

Corresponding percentage of axial/lateral occlusal forces and boundary condition was shown in the solid model column. FE: Finite element

All materials included cortical, cancellous bones, bone graft, reconstruction implant/screws, and dental implants defined with linear elastic and isotropic properties and adopted from the relevant literature (Table 6).

Weighted topology optimization was performed for structures to define lightweight and structural strengthening characteristics for the B/C/A+B reconstructed implant<sup>[11]</sup>. The reconstructed implant core considered the scoping region for optimizing the process topology with stress constraints to find the objective function for minimizing the core volume. Two load conditions (100 N) were defined as uniform multiple axial and oblique (45° incline to the tooth axis from buccal to lingual) contacts on the teeth according to different segments applied on the three models to evaluate the mechanical responses. We assumed 70% of the C segment would be subjected to oblique occlusal forces and 30% would be subjected to axial occlusal forces due to the chewing situation in the anterior region having more emphasis on lateral force. On the contrary, 40% of the B and A+B segments would be subjected to oblique occlusal forces and 60% would be subjected to axial occlusal forces because the

**Table 6.** Elastic modulus and Poisson's ratios of all materials simulated using finite element analysis.

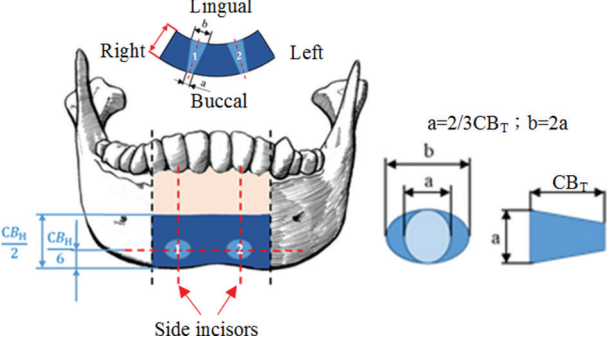
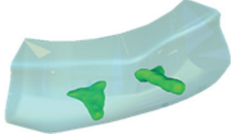


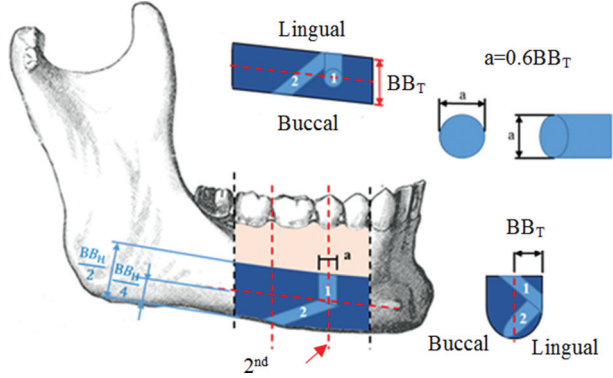
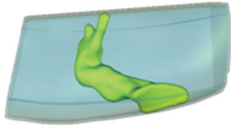

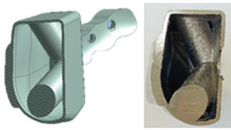
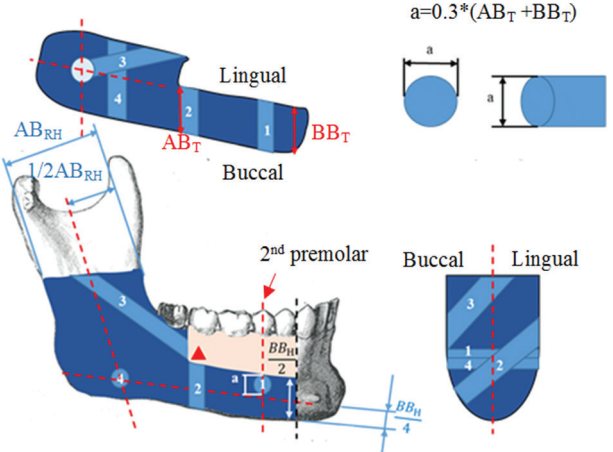
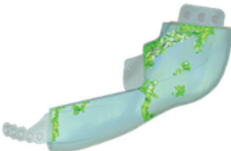

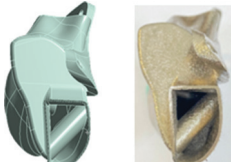
Material	Elastic modulus	Poisson's ratio	Reference
Cortical bone	13,700 MPa	0.30	[3,10,11,17]
Cancellous bone	1370 MPa	0.30	
Reconstructed implant and fixation screw (Ti6Al4V)	110 GPa	0.35	
Bone graft	13,700 MPa	0.3	
Dental implant	110 GPa	0.35	

axial bite force was heavier than the lateral force in the posterior region<sup>[11,19,20]</sup> (Table 5). Nodes on the condyle were constrained in all directions in all models to prevent movement as the boundary conditions to perform the weighted topology optimization<sup>[9]</sup> (Table 5). The final weighted topology optimization result summed up the compliance of each model for all load cases. Each of these

segments was multiplied by the respective load (axial/oblique) weight coefficients<sup>[11]</sup>. Finally, three models with

internal optimal core structures were obtained using a model smoothing procedure (Table 7).

**Table 7.** Parametric design for internal supporting beam of C, B and A+B reconstructed implants.

Area	Parametric design for internal beam structure of the 3D Printing implant	Topology result (up), simply noted (middle) and parametric design model structures (CAD and AM) (down)
C		   <p style="text-align: center;">CAD      AM</p>
B		   <p style="text-align: center;">CAD      AM</p>
A+B		   <p style="text-align: center;">CAD      AM</p>

AM: Additive manufacturing, CAD: Computer aided design

The core structure of C/B/A+B segments calculated using weighted topology optimization can be simplified into a parametric equation based on the teeth positions and the size of the bone segment to define the position and size of the internal supporting beam structures. Taking area C as an example, a cross-section of the two supporting beams (a and b sizes at the **Table 7** upper part) was set as a circle to ellipse from the buccal to lingual side. The corresponding center position was located at the interaction of the side incisor axis on the left/right side and one-sixth of the C segment height and extended from the buccal side to the lingual side. The cross-sectional beam size at the buccal/lingual side can be calculated from the C segment width (**Table 7**). The internal supporting beam structure of the B/A+B segments was also parametrically defined by the bone width/height and the teeth position in the corresponding bone segment (**Table 7**).

Three FE restored mandibular defect models included corresponding remaining mandible and graft bones with dental implants generated sequentially based on the simplified internal support beam structure of the C/B/A+B reconstructed implants. Accommodated element and node numbers of three models are listed in **Table 5**. The loading and boundary conditions used in FE analysis are the same as those used in weight topology optimization analysis. Volume and the von Mises stress of the reconstructed implant and the maximum principal stress of the remaining bone in these three models were calculated to understand the model simplification efficiency after performing FE simulations.

#### 2.4. AM reconstructed implant and biomechanical testing

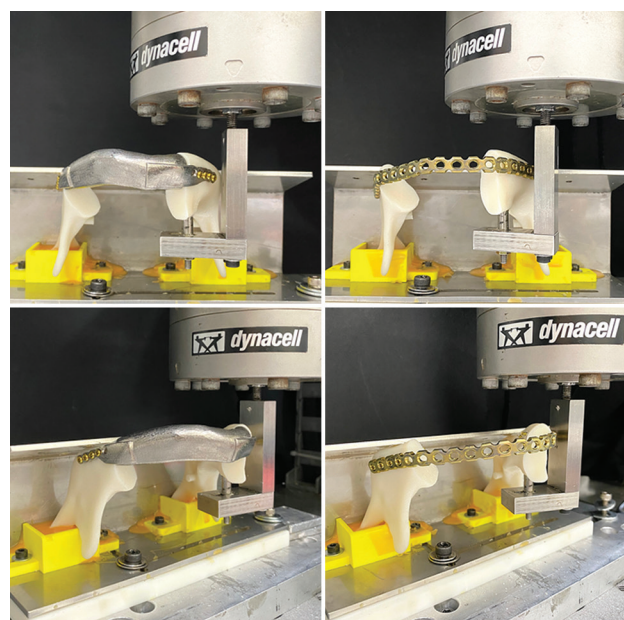
Five reconstructed implant included C, B, A+B, B+C, and B+C+B segments were manufactured using the metal AM technique. The internal supporting beam structures of B, C, and A+B were designed according to results of previous weight topology optimization, and the corresponding structure of B+C/B+C+B segments was designed using a combination of C and B designs. A metal 3D printer (AM400, Renishaw, Gloucestershire, UK) with titanium alloy powder (Ti6Al4V powder with average grain size of 30  $\mu\text{m}$ ) was used to manufacture five reconstructed implants. The 3D printing machine was operated with a laser power of 400 W, a scanning rate of 0.6 m/s, and exposure time of 125 s with a spot diameter of 70  $\mu\text{m}$ , and an accuracy of  $\pm 25$   $\mu\text{m}$  in the laser beam movement and positioning. Implants were then acid etched to remove residual sandblast particles and cleaned using ultrasonic oscillations<sup>[8,11]</sup>. The corresponding five remaining mandible bone models were duplicated in acrylonitrile butadiene styrene (ABS-P430; Stratasys, Ltd., Minnesota, USA) using a 3D printer (Dimension 1200es SST, Stratasys, Ltd., Minnesota, USA) (2<sup>nd</sup> column of **Table 8**).

The biomechanical test samples were divided into the reconstructed implant ( $n=3$ ) and traditional commercial bone plate group ( $n=3$ ) (control group). The remaining mandibular ABS bone model of each defect segment<sup>[21]</sup> and the corresponding AM reconstructed implant and the control group (traditional bone plate; UniLock 2.4; Synthes, Umkirch, Germany) were fixed with a bone screw (Tandry Locking Bone Plate System  $\psi 2.4$  mm L18 mm, All Micro Precision Co., Ltd., Taiwan) (2<sup>nd</sup> column of **Table 8**). All tested samples were clamped onto a test machine (Instron E3000, Instron, Canton, MA, USA) with an axial load cell according to **Figure 3**. Each test sample was fixed upside down on the machine and the condyle head fixed in an embedded resin block to apply a reaction force to the mandible angle according to the Wiebke Schupp test method and the work of other scholars<sup>[21]</sup>.

A 20~200 N dynamic cyclic load was applied to the 2<sup>nd</sup> molar on the opposite side of the defect segment to perform fatigue testing at a frequency of 3 Hz (**Figure 3**). The test stopped when the sample fractured or received 250,000 times the dynamic load which simulated the actual occlusal situation 6 months after the clinical surgery<sup>[21]</sup>. The remaining mandible displacement was recorded by the Instron testing machine unless the test sample was damaged during the fatigue experiment to stop the testing.

### 3. Results

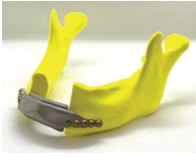

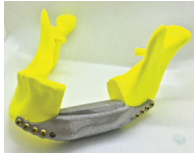



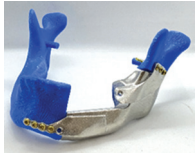

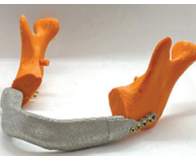

According to the calculation results from 105 patients, the V value was found between 13.71 and -25.74



**Figure 3.** Biomechanical fatigue test illustration for B+C restored mandibles with AM reconstructed implants and bone plate. Left: AM reconstructed implants front (up) and ISO (down) views. Right: bone plate front (up) and ISO (down) views.



**Table 8.** Results of biomechanical fatigue tests included displacements of 3D Printing reconstructed implants and failure pattern of commercial plate.

Segment	Failure pattern of mandibular defect with using AM implant	Displacement of using AM implant (mm)		Failure pattern of mandibular defect of using bone plate	Displacement of using traditional bone plate and cyclic load number (times)	
		Pass	Ave.		Pass	Ave.
C		Pass	2.05		186769	Condyle head fracture
			2.41		189412	Screw head damage
			1.78		Pass	2.38
		Ave.	2.26		Ave.	
		SD	0.31		SD	
B		Pass	2.61		120546	Condyle head fracture
			2.16		125000	Bone plate fracture
			2.01		82000	Bone plate fracture
		Ave.	2.26		Ave.	
		SD	0.31		SD	
B + C		Pass	2.04		61661	Condyle head fracture
			3.81		75450	Condyle head fracture
			2.18		54773	Condyle head fracture
		Ave.	2.68		Ave.	
		SD	0.98		SD	
A + B		Pass	2.85		85440	Condyle head fracture
			2.58		124834	Condyle head fracture
			2.49		58656	Condyle head fracture
		Ave.	2.64		Ave.	
		SD	0.19		SD	
B + C + B		Pass	2.20		29585	Bone plate fracture
			2.72		26032	Bone plate fracture
			1.78		38680	Bone plate fracture
		Ave.	2.23		Ave.	
		SD	0.47		SD	

(Table 2). The five cases with the largest V value selected from 105 patients were the cases with the weakest mandible structural strength and their corresponding V and SDZ values were found between 12.14 and 17.51 and 0.78 and 1.06, respectively. The worst mandible structural strength case was found as No. 3 in Table 3 when we set V with largest and SDZ with smallest values and corresponding values were 13.71 and 0.66, respectively.

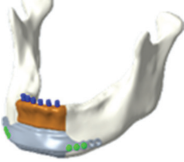

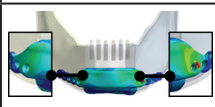
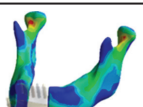

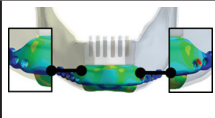
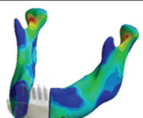
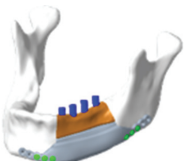
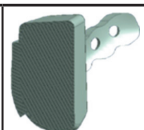
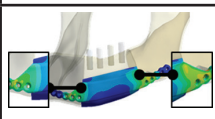
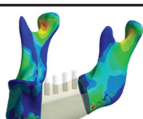
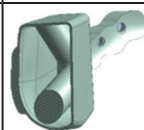
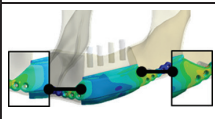
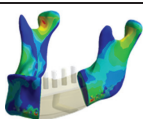
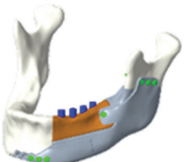

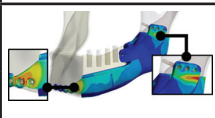
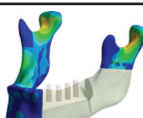

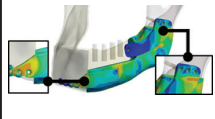
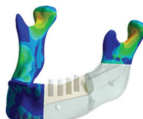
The weighted optimization analysis result indicated that the internal support beam structure within the reconstructed implants of C, B, and A+B can be obtained, and the size and position of the supporting beam structures can be designed parametrically through corresponding bone length, width, and height. For example, the support beam structures in the C reconstructed implant were two pillars with an elliptical cross-sectional area with and parametric expressed its position and size through side incisor axis and bone height of the C segment (Table 7). Detailed sizes and positions of supporting beam structures

in the B and A+B reconstructed implants can also be defined using a similar method as found in Table 7.

The FE analysis results found that the percentage variation in weight between the parametric designed implants and original core solid implants in the C, B, and A+B was reduced by 54.3%, 63.7%, and 69.7%, respectively (Table 9). Compared with the maximum von Mises stress of the reconstructed implants, the C segment increased by 5.3%, while the B and A+B areas reduced by 8.2% and 5%, respectively. All stress concentration areas were at the junction between the wings and the reconstructed implant. Although stress value increased slightly in the C segment, the stress value was still far from the material failure threshold. However, the variation in the remaining bone stress was found from -17% to 0% (Table 9).

The C/B/A+B/B+C/B+C+B testing samples included reconstructed implant with the remaining bones shown in the 2<sup>nd</sup> column of Table 8. The internal supporting beam structure of the C/B/A+B segments can

**Table 9.** Results of finite element simulations of mandibular large defect repaired with solid and parametric reconstruction implants.

			Weight (g)	Maximum von Mises Stress (MPa) (implant)		Maximum principal stress (MPa) (remaining bone)			
Segment C 	Solid model 		27.95		Max. 30 30 25 20 15 12 10 5 2.5 (MPa)	18.45		Max. 100 100 80 60 30 10 5 3 1 (MPa)	51
	Parametric model 		12.76			19.43			50
Variation between solid and parametric model			-54.3%			5.3%			-2%
Segment B 	Solid model 		45.08		Max. 250 250 200 150 100 50 30 15 5 (MPa)	235.61		Max. 100 100 80 60 30 10 5 3 1 (MPa)	68.14
	Parametric model 		16.35			230			56.59
Variation between solid and parametric model			-63.7%			-8.2%			-17%
Segment A+B 	Solid model 		85.91		Max. 100 100 90 80 70 60 50 40 30 (MPa)	285		Max. 100 100 80 60 30 10 5 3 1 (MPa)	88.6
	Parametric model 		26			271			88.5
Variation between solid and parametric model			-69.7%			-5%			0%

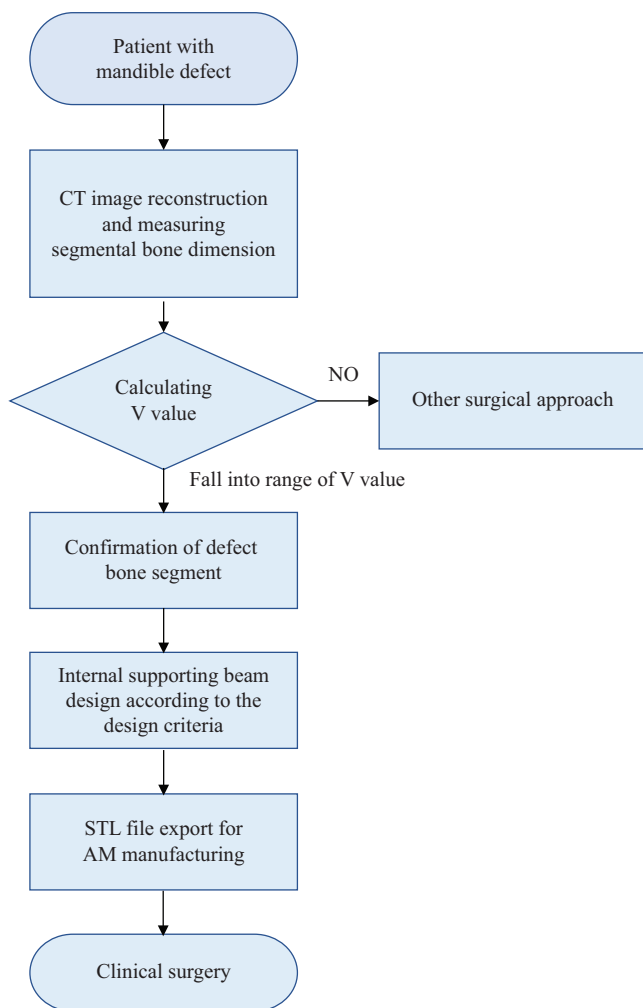
also be found in **Tables 7** (3<sup>rd</sup> column) and **9** (3<sup>rd</sup> column). The biomechanical fatigue test results are listed and shown in **Table 8**. All cases using the AM reconstructed implant can pass the 250,000 dynamic load level without causing damage to the samples. However, the damaged locations can be found in the condyle head of the mandible, bone plate fracture, and bone screw loosening for the five cases of C/B/A+B/B+C/B+C+B when using traditional bone plates.

#### 4. Discussion

Oral cancer-induced continuity defect in the mandible is a very troublesome or complicated disease in Asia, especially in Taiwan. Effectively reconstructing the

defective mandible is an important surgery. The long-term survival rate for this surgery has gradually improved in recent years due to the advent of chemotherapy and radiotherapy target drugs. Nevertheless, further integrated engineering technologies, such as image processing, CAD, FE analysis, and optimization analysis for structural design and AM manufacturing to improve the appearance and prosthesis requirements for large mandibular reconstructed implants are necessary.

According to FDA regulations, it is not possible to perform SE fatigue test comparison for a single mandible defect region for a specific patient. To enable specific patient clinical application design criterion for reconstructed implants in the future and meet the



**Figure 4.** Flowchart of mandibular defect reconstruction in adherence with our design criteria.

mechanical SE comparison, this study establishes an effective mandible image database and identified the worst mandible structural strength to perform segmental lightweight structure optimization analysis. The segmental lightweight structure can withstand the occlusal force for further dental implant/prosthesis considerations. The design criteria developed in this study can be subsequently applied to the clinic according to **Figure 4**. The patient's mandible segmental dimension characteristics can be measured using CT images according the definition in **Table 1** and obtained the V value through Equation 1. The V value was used as a simplified value to express the mandible structural strength. Its positive and negative values were derived from the bending stress of the mandible. When the bending stress ( $\sigma$ ) of the cantilever beam was calculated, a positive correlation was found between  $\sigma$  and the LB of the mandible, and a negative correlation was found between HB and TB. The cantilever beam theory proves

that longer mandibles have higher bending stress ( $\sigma$ ) and are more prone to damage. When calculating the V value, the height and thickness values should be preceded by a negative sign, indicating that  $\sigma$  is negatively correlated with HB and TB. A large V value indicates a dangerous mandible structure (worst case) because the mandible is subjected to more bending stress ( $\sigma$ ). The V value result was found from the range between 13.71 and  $-25.74$ , meaning that if the V value of another defected mandible falls in this range, it can be repaired using the design criteria proposed in this study.

Due to the size and position of the internal supporting beams for various reconstructed implants, parametrically design using the corresponding patient-specific segmental bone thickness, height, and teeth position, patient-specific reconstructed implants with lightweight structure can be obtained directly according to our developed design criteria and exported for AM (**Table 7**). The internal support beam design for segmental reconstructed implant C was described in section 2.3. The internal two support beams of reconstructed implant B were oblique cylinders and beam 1 extended from the implant surface at the 2<sup>nd</sup> premolar axis to the lingual side with a quarter of the bone height. Beam 2 extended from the end of beam 1 to the buccal side with the bottom of the implant at the distal 1<sup>st</sup> molar margin. In addition, there were four beam supporting beams within the reconstructed implant A+B, beams 1 and 4 were cylinders from lingual to buccal sides with positions at the 2<sup>nd</sup> premolar center with a height of  $(BB_H/4+a/2)$  at the intersection of  $1/2 AB_{RH}$  and  $BB_H/4$  axis, respectively. Beams 2 and 3 were oblique cylinders, with beam 2 extended from the top surface turning point of the implant at the lingual side to the buccal side with the bottom surface of the implant at the axis of the 2<sup>nd</sup> molar and beam 3 extended from the half of  $AB_{RH}$  of the top surface of the implant to the buccal side at the implant turning point. Other internal support beam bone segments for B+C and B+C+B can then be defined using a combination of B and C bone segments (**Table 7**).

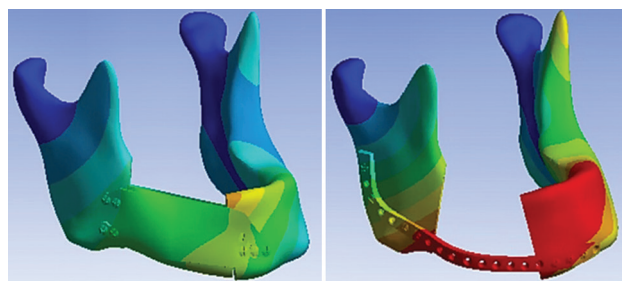
The reconstructed implant design based on our criteria must consider the upper space to allow further bone grafts to have dental implants with prosthesis. The thickness must also consider the space for soft-tissue flap. However, a dental implant with prosthesis still cannot be designed and manufactured together in this study because it easily causes bacterial infection if the soft tissue cannot completely cover the metal implant<sup>[22]</sup>. The dental implant with prosthesis can be planned and printed before surgery if the contact area between the mucosal tissue and the metal can be effectively treated antibacterial medicines or the relevant AM material is developed.

At present, relevant research that can be used to verify the results of the current study is unavailable. However, there were similar studies on mandibular reconstruction

implant structure optimization<sup>[8,9]</sup>. These studies also advocated the importance of “custom-made” personalized implants that can be fabricated using the AM technique. In addition to reducing the reconstruction implant weight, performing implant structure optimization analysis also reduces the stress shielding that might cause bone resorption and eventual failure<sup>[23]</sup>. The current analysis results showed that the reconstructed implant weights in different segments can be reduced by at least 50% through the lightweight optimization structural design. This result was consistent with the study by Cheng *et al.* who produced a titanium canine mandibular implant that possessed a personalized external shape for appearance recovery and structural optimization and a weight reduction of 37.2%<sup>[8]</sup>. However, the maximum stress values of the reconstructed implant and the remaining bone were not obviously reduced in this study. The stress values were, however, far lower due to the materials’ ultimate strength. This is still within the acceptable range. The stress concentrations of the reconstructed implants were also noted the same as on the connected fixation wing and fixation screws with other studies. This inferred that implant failure can occur due to high stress concentration on the screws in the fixation unit and implied that the fixation wing can be improved for further design<sup>[8]</sup>.

The biomechanical fatigue test results indicated that all mandibular continuity defects using AM reconstructed implants based on our design criteria can pass the 250,000 cyclic load test, that is, survival in actual occlusal situations for about 6 months after clinical surgery. However, failure tests with mandibular condyle head fracture, bone plate fracture, or bone screw loosening were found corresponding with mandibular continuity defects using traditional bone plate. This phenomenon was because the traditional bone plate cannot provide enough stiffness to maintain stability for the restored mandible, causing it to become strongly distorted when receiving repeated occlusal force. Taking the B segment as an example for FE analysis, the simulated result found that the twist displacement of the mandibular defect used with traditional bone plate was much larger than that used in the AM reconstructed implant (**Figure 5**). In addition, an axial force state induced the bending moment effect on the reconstructed implant only when applied on the mandible of the current biomechanical test. Standard 4-point bending fatigue tests based on ASTM F382 testing method need to be performed in the future to compare the implant mechanical strength between different AM reconstructed implants and traditional bone plate to comply with the FDA’s SE functional test comparison for marketing<sup>[23]</sup>.

The mandibular bone CT image database was constructed using images of only 105 patients in this study. The current most important task is to apply our reconstructed implant for restored severe mandibular defect in clinical



**Figure 5.** Finite element displacement comparison between B segmental mandible defect restored with reconstructed implants and bone plate.

trials. The number of mandible CT images in the database can be gradually expanded to include patients outside of Taiwan after the clinical application of our reconstructed implant is successful. Following up with the developed technique in this study, remote design, and manufacture of the reconstructed implant can be performed through the medical network for clinical treatment.

## 5. Conclusions

This study developed a design criterion for patient-specific reconstructed implants with lightweight structural optimization for various mandibular continuity defects. The sizes and positions of the internal support beams for the reconstructed implant are defined parametrically through corresponding segmental bone length, width, and height. Biomechanical fatigue testing validated that all mandibular continuity defects using the AM reconstructed implant can pass cyclic dynamic loads. Condyle head, bone plate fractures, and bone screw loosening can be found in restored mandibular defects using bone plates.

## Acknowledgments

Authors would like to appreciate Anji Technology Co., Ltd., for assistant in metal 3DP manufacture.

## Funding

This study is supported in part by MOST project 108-2622-E-010-001-CC2 and 108-2622-B-010-005, Taiwan.

## Conflict of interest

The authors declare no conflicts of interest.

## Authors contributions

All authors have made substantial contributions to conception and design of the study. Y.T. Wang, C.M. Chang, and W.H. Tsai have been involved in data collection and data analysis. C.L. Lin, Y.T. Wang, and

C.H. Wu were involved in data interpretation, drafting the manuscript and revising it critically, and given final approval of the version to be published. All authors read the published manuscript version and agreed.

## References

- Patel A, Harrison P, Cheng A, et al., 2019, Fibular Reconstruction of the Maxilla and Mandible with Immediate Implant-Supported Prosthetic Rehabilitation: Jaw in a Day. *Oral Maxillofac Surg Clin North Am*, 31:369–86. <https://doi.org/10.1016/j.joms.2019.03.002>
- Toure G, Gouet E, 2019, Use of a 3-Dimensional Custom-Made Porous Titanium Prosthesis for Mandibular Body Reconstruction with Prosthetic Dental Rehabilitation and Lipfilling. *J Oral Maxillofac Surg*, 77:1305–13. <https://doi.org/10.1016/j.joms.2018.12.026>
- Qin M, Liu Y, Wang L, et al., 2015, Design and Optimization of the Fixing Plate for Customized Mandible Implants. *J Craniomaxillofac*, 43:1296–302.
- Stoor P, Suomalainen A, Mesimäki K, et al., 2017, Rapid Prototyped Patient Specific Guiding Implants in Critical Mandibular Reconstruction. *J Craniomaxillofac Surg*, 45:63–70. <https://doi.org/10.1016/j.jcms.2016.10.021>
- Lee S, Kim HG, Ham MJ, et al., 2018, Custom Implant for Reconstruction of Mandibular Continuity Defect. *J Oral Maxillofac Surg*, 76:1370–6.
- Yusa K, Yamanouchi H, Yoshida Y, et al., 2017, Evaluation of Quality of Life and Masticatory Function in Patients Treated with Mandibular Reconstruction Followed by Occlusal Rehabilitation with Dental Implants: A Preliminary Report. *J Oral Maxillofac Surg Med Pathol*, 29:499–503. <https://doi.org/10.1016/j.ajoms.2017.06.004>
- Liu YF, Fan YY, Jiang XF, et al., 2017, A Customized Fixation Plate with Novel Structure Designed by Topological Optimization for Mandibular Angle Fracture Based on Finite Element Analysis. *Biomed Eng Online*, 16:131–47. <https://doi.org/10.1186/s12938-017-0422-z>
- Cheng K, Liu Y, Yao C, et al., 2019, A Personalized Mandibular Implant with Supporting and Porous Structures Designed with Topology Optimization—a Case Study of Canine. *Rapid Prototyp J*, 25:417–26. <https://doi.org/10.1108/rpj-11-2017-0231>
- Pinheiro M, Alves JL, 2015, The Feasibility of a Custom-Made Endoprosthesis in Mandibular Reconstruction: Implant Design and Finite Element Analysis. *J Craniomaxillofac Surg*, 43:2116–28. <https://doi.org/10.1016/j.jcms.2015.10.004>
- Moiduddin K, Hammad Mian S, Alkhalefeh H, et al., 2019, Digital Design, Analysis and 3D Printing of Prosthesis Scaffolds for Mandibular Reconstruction. *Metals*, 9:569. <https://doi.org/10.3390/met9050569>
- Li CH, Wu CH, Lin CL, 2020, Design of a Patient-Specific Mandible Reconstruction Implant with Dental Prosthesis for Metal 3D Printing Using Integrated Weighted Topology Optimization and Finite Element Analysis. *J Mech Behav Biomed Mater*, 105:103700. <https://doi.org/10.1016/j.jmbbm.2020.103700>
- Kumar BP, Venkatesh V, Kumar KA, et al., 2016, Mandibular Reconstruction: Overview. *J Maxillofac Oral Surg*, 15:425–41. <https://doi.org/10.1007/s12663-015-0766-5>
- Hara D, 2016, Bone Bonding Strength of Diamond-Structured Porous Titanium-Alloy Implants Manufactured Using the Electron Beam Melting Technique. *Mater Sci Eng C*, 59:1047–52. <https://doi.org/10.1016/j.msec.2015.11.025>
- Taniguchi N, 2016, Effect of Pore Size on Bone Ingrowth into Porous Titanium Implants Fabricated by Additive Manufacturing: An *In Vivo* Experiment. *Mater Sci Eng C*, 59:690–701. <https://doi.org/10.1016/j.msec.2015.10.069>
- Premarket Notification, 2018, No. K173039, 510(K) Premarket Notification, FDA, U.S., p1–11.
- Beer FP, Johnston ER Jr., DeWolf JT, et al., 2017, Mechanics of Materials. 7<sup>th</sup> ed., Ch. 4. New York, United States: McGraw-Hill.
- Lin CL, Wang JC, Chang WJ, 2008, Biomechanical Interactions in Tooth-Implant-Supported Fixed Partial Dentures with Variations in the Number of Splinted Teeth and Connector Type: A Finite Element Analysis. *Clin Oral Implants Res*, 19:107–17. <https://doi.org/10.1111/j.1600-0501.2007.01363.x>
- Narra N, Valášek J, Hannula M, et al., 2014, Finite Element Analysis of Customized Reconstruction Plates for Mandibular Continuity Defect Therapy. *J Biomech*, 47:264–8. <https://doi.org/10.1016/j.jbiomech.2013.11.016>
- Warreth A, 2015, Fundamentals of Occlusion and Restorative Dentistry. Part I: Basic Principles. *J Ir Dent Assoc*, 61:201–8.
- Al Qassar SS, Mavragani M, Psarras V, et al., 2016, The Anterior Component of Occlusal Force Revisited: Direct Measurement and Theoretical Considerations. *Eur J Orthod*, 38:190–6. <https://doi.org/10.1093/ejo/cjv028>

21. Schupp W, Arzdorf M, Linke B, *et al.*, 2007, Biomechanical Testing of Different Osteosynthesis Systems for Segmental Resection of the Mandible. *J Oral Maxillofac Surg*, 65:924–30.  
<https://doi.org/10.1016/j.joms.2006.06.306>
22. Lee CT, Huang YW, Zhu L, *et al.*, 2017, Prevalence of Peri-Implantitis and Peri-Implant Mucositis: Systematic Review and Meta-Analysis. *J Dent*, 62:1–12.  
<https://doi.org/10.1016/j.jdent.2017.04.011>
23. Long M, Rack HJ, 1998, Titanium Alloys in Total Joint Replacement-A Materials Science Perspective. *Biomaterials*, 19:1621–39.  
[https://doi.org/10.1016/s0142-9612\(97\)00146-4](https://doi.org/10.1016/s0142-9612(97)00146-4)
24. Standard ASTM, 2017, F382-17 Standard Specification and Test Method for Metallic Bone Plates, *ASTM Int*, 13:1–40.

#### **Publisher's note**

Whoice Publishing remains neutral with regard to jurisdictional claims in published maps and institutional affiliations.